Global systematics of octupole excitations in even-even nuclei

L. M. Robledo and G. F. Bertsch

Phys. Rev. C **84**, 054302 — Published 1 November 2011

DOI: 10.1103/PhysRevC.84.054302

Global systematics of octupole excitations in even-even nuclei

L.M. Robledo*

Departamento de Física Teórica, Módulo 15,

Universidad Autónoma de Madrid, E-28049 Madrid, Spain

G.F. Bertsch

Institute for Nuclear Theory and Dept. of Physics, Box 351560,

University of Washington, Seattle, Washington 98915, USA

Abstract

We present a computational methodology for a theory of the lowest octupole excitations applicable to all even-even nuclei beyond the lightest. The theory is the well-known generator-coordinate extension (GCM) of the Hartree-Fock-Bogoliubov self-consistent mean field theory (HFB). We use the discrete-basis Hill-Wheeler method (HW) to compute the wave functions with an interaction from the Gogny family of Hamiltonians. Comparing to the compiled experimental data on octupole excitations, we find that the performance of the theory depends on the deformation characteristics of the nucleus. For nondeformed nuclei, the theory reproduces the energies to about ± 20 % apart from an overall scale factor of ≈ 1.6. The performance is somewhat poorer for (quadrupole) deformed nuclei, and for both together the dispersion of the scaled energies about the experimental values is about ± 25 %. This compares favorably with the performance of similar theories of the quadrupole excitations. Nuclei having static octupole deformations in HFB form a special category. These nuclei have the smallest measured octupole excitation energies as well as the smallest predicted energies. However, in these cases the energies are seriously underpredicted by the theory. We find that a simple two-configuration approximation, the Minimization After Projection method, (MAP) is almost as accurate as the full HW treatment, provided that the octupole-deformed nuclei are omitted from the comparison. This article is accompanied by a tabulation of the predicted octupole excitations for 818 nuclei extending from drip-line to drip-line, computed with several variants of the Gogny interaction.

*Electronic address: `luis.robledo@uam.es`; URL: `http://gamma.ft.uam.es/robledo`

I. INTRODUCTION

The octupole excitations of nuclei have been well-studied theoretically on a case-by-case basis but there has never been a global study for a fixed Hamiltonian and well-defined computational methodology. Such studies are important for several reasons. Seeing the systematic trends, one can better assess the deficiencies in the Hamiltonian or the underlying theory, which could hopefully lead to improvements on both sides. Also, the predictive power of the theory with the given Hamiltonians can be measured by the comparison to a large body of nuclear data. In this work we carry out a study of this kind using the Hartree-Fock-Bogoliubov (HFB) approximation extended by the Generator Coordinate Method (GCM). Earlier studies of the octupole degree of freedom using this and similar methods are in Refs. [1–6]. A competing methodology is based on the quasiparticle random phase approximation; recent application to octupole modes may be found in Refs. [7–9]. For a general review of the theory of octupole deformations and collective excitations, see Ref. [10].

A global theory not only needs to treat the consequences of static octupole deformations in HFB ground states but also to treat the more ordinary situation where the degree of freedom appears more as a collective vibration of a symmetric HFB ground state. The latter is typically treated by RPA or QRPA [7–9], but the most of the studies consider a small body of nuclei chosen by considerations emphasizing one characteristic or another, for example semi-magic isotope chains. Our study is the first to encompass not only magic and semi-magic ordinary nuclei, but the quadrupole- and octupole-deformed nuclei as well. This follows in spirit the studies of the nuclear quadrupole degrees of freedom in Refs. [11, 12]. We mention that our GCM coordinate is a one-dimensional variable labeled by the mass octupole moment. A two-dimensional treatment of the octupole deformations treating the quadrupole deformation as a separate degree of freedom is important in the theory of fission [13], and is likely to play a role in spectroscopy as well [14].

The HFB fields and quasiparticle wave functions are assumed to have the following symmetries: time reversal, axial symmetry, and the z -component of isospin. We can only consider even-even nuclei under these restrictions. The restriction to axial symmetry is harmless in spherical nuclei, but for deformed nuclei it causes two problems. The first is that theory only treats the $K = 0$ excitations of deformed nuclei. As we will see, some of the identified octupole excitations very likely have nonzero K quantum number. The

second difficulty that arises with deformed nuclei is that angular momentum is not a good quantum number of the HFB/GCM wave function. On a practical level, we shall compare the calculated excitation energies with the spectroscopic $0^+ \to 3^-$ transitions, assuming that the rotational inertias can be neglected.

The calculations are carried with Gogny's form of the interaction in the Hamiltonian. Specific results for the D1S interaction will be presented below. That interaction has been well-tested in many HFB calculations and also gives good results in (Q)RPA [15] and GCM extensions of HFB [16]. Results for other Gogny interactions are provided in the supplementary material accompanying this article.

II. IMPLEMENTING THE GCM

A. GCM

In the GCM, an external field is added to the Hamiltonian to generate a set of mean-field configurations to be taken as a basis for the HW minimization. We take for the generating field the mass octupole operator, $\hat{Q}_3 = \sqrt{\frac{4\pi}{7}} r^3 Y_0^3(\hat{r}) = z^3 - \frac{3}{2} z(x^2 + y^2)$. We label the solutions of the HFB equations in the presence of the field $\lambda \hat{Q}_3$ by the expectation value of $\hat{Q}_3$,

$$\langle q|\hat{Q}_3|q\rangle = q. \tag{1}$$

For convenience, we will use the nominal value of β_3 instead of q in discussing the wave functions. These are related by the formula $q = \sqrt{9/28\pi}(1.2)^3 A^2 \beta_3$. We also fix the (average) center-of-mass of the nucleus at the origin with the constraint $\langle|\hat{z}|\rangle = 0$ to avoid a spurious octupole moment associated with the position of the nucleus. For each octupole constrained wave function the quadrupole moment is determined self-consistently to minimize the HFB energy.

The GCM wave function is constructed by combining the configurations $|q\rangle$ to build a correlated wave function $|\sigma\rangle$. This is expressed formally in the GCM as an integral over configurations

$$|\sigma\rangle = \int dq\, f_\sigma(q)|q\rangle. \tag{2}$$

The function f in Eq. (2) is to be determined by applying the variational principle to the

expression

$$E = \frac{\langle\sigma|H|\sigma\rangle}{\langle\sigma|\sigma\rangle}. \tag{3}$$

While Eqs. (2) and (3) define the GCM formally, further approximations are required to arrive at a well-defined computational methodology. One way common in the literature is to keep the formal integral Eq. (2) and use the Gaussian overlap approximation to calculate the matrix elements in Eq. (3), as was done in Ref. [12] to map the quadrupole deformation onto a collective Hamiltonian, and in Ref. [17] for the octupole degree of freedom. A quite different way is the *discrete basis Hill-Wheeler* method, first carried out for the octupole excitations in Ref. [1]. This method, which we will follow here, approximates the integral using a discrete set of configurations. The minimization of the GCM energy is equivalent to solving the matrix eigenvalue equation

$$\sum_j \langle q_i|H|q_j\rangle c_j = E\langle q_i|q_j\rangle c_j. \tag{4}$$

The states will have good parity if the basis is reflection symmetric, i.e. if both $|-q_i\rangle$ and $|q_i\rangle$ are in the basis.

For either method one needs the overlap integrals between configurations $\langle q|q'\rangle$, the matrix elements of the Hamiltonian $\langle q|H|q'\rangle$ and the matrix elements of one-body operators such as $\langle q|\hat{Q}_3|q'\rangle$. The basic overlap integral is computed with the Onishi formula[18]. The matrix elements of one-body and two-body operators are then evaluated using the generalized Wick's theorem[19]. Unfortunately, the Gogny interaction cannot be expressed in this way due to its $\rho^{1/3}(\vec{r})$ density dependence. This gives rise to well-known ambiguities in treating the interaction as a Hamiltonian in a multiconfiguration space. Of the various prescriptions available, we use the "mixed density" method. Here the ρ in the $\rho^{1/3}$ factor is replaced by $\rho_{qq'}(\vec{r})$ given by

$$\rho_{qq'}(\vec{r}) = \frac{\langle q|\hat{\rho}(\vec{r})|q'\rangle}{\langle q|q'\rangle} \tag{5}$$

and the resulting $\vec{r}$-dependent interaction is evaluated in the usual way. The mixed-density prescription was introduced in Ref [20] and first applied to parity-projected HFB as "Prescription 2" in Ref [3]. It is consistent with the mean field limit and is a scalar under symmetry transformations [21]. Another prescription which seems plausible at first sight is to use the projected density for $\rho^{1/3}$. However, this gives unphysical results for octupole deformations[22].

While the configurations $|q\rangle$ constructed with the octupole constraint have mixed parity, the HW solutions restore the parity quantum number, as was discussed above. In effect, the parity projection needed to calculate spectroscopic properties can be obtained from the HW minimization without any extra effort. However, as a practical matter, it is easier to define the parity operator in the harmonic oscillator basis and use it to construct $|-q\rangle$ from $|q\rangle$ thus avoiding a separate HFB minimization for the $-q$ configuration.

The HW states of interest are the lowest lying even- and odd-parity states of the spectrum, which we call $|e\rangle$ and $|o\rangle$. Taking them to be normalized, the energies of ground state E_e, the odd parity state E_o, and the excitation energy difference E_3 are given by

$$E_e = \langle e|H|e\rangle; \quad E_o = \langle o|H|o\rangle; \quad E_3 = E_o - E_e \tag{6}$$

We follow the usual procedure to solve the matrix equation Eq. (4), using if necessary the singular value decomposition of the overlap matrix to avoid difficulties with an overcomplete space.

One first diagonalizes the overlap matrix and transforms all of the matrices to the diagonalized basis. Often there will be vectors which very small norms and the basis is truncated to exclude them when the norms are less than a certain value n_{min}. The Hamiltonian is diagonalized in this basis, called the collective space, to give the HW energies. The eigenvectors of the Hamiltonian are used to calculate matrix elements of other operators between energy eigenstates.

The main problem with the discrete Hill-Wheeler method is that the calculated values cannot be considered reliable unless both the range of deformations has been fully covered and that the singular value decomposition has been set to a robust truncation. For most of the nuclei, we shall take as a basis the set of β_3 from -0.5 to +0.5 in steps of 0.025. For lighter nuclei, the range is extended from -1.2 to +1.2. The calculations are carried out as a function of the dimension N_{basis} of the singular-value truncation. There is generally a broad range of N_{basis} for which the excitation energies have converged to some value; we take the value on this plateau as the HW result. An example is shown in detail in the next section.

The computation of the HW starting matrices is not trivial, requiring $N(N+1)/2$ Hamiltonian matrix elements for a basis size N. While this is not an important issue here, if one were to attempt GCM calculations in more than one variable, the number of states N_{basis} could be large. It is therefore of interest to investigate the accuracy of simpler approximations

using fewer configurations. One of the simplest treatments is to take two configurations, $|q_e\rangle$ and $|q_o\rangle$, for the even-parity and odd-parity state, respectively. The values of q are chosen to minimize the projected energies of the configuration. We follow Ref. [11] calling this the Minimization After Projection (MAP) procedure. The deformations and energies at the minima are denoted β_{3p}, E_p and β_{3m}, E_m for the two projected states. The MAP excitation energy is defined as

$$E_3^{MAP} = E_m - E_p \tag{7}$$

One last general point of the computational procedure needs to be mentioned. While the individual HFB configurations are constructed with the desired proton and neutron particle numbers, the mixed configurations in the HW wave function may have slightly different expectation values of N and Z. The energy depends strongly on $\langle N\rangle$ and $\langle Z\rangle$, and changes must be corrected for. We do this by adding to the HW Hamiltonian the term $\lambda_p(\hat{Z} - Z) + \lambda_n(\hat{N} - N)$, where $\lambda_{p,n}$ are the nucleus' chemical potentials at β_{3p} [20].

B. HFB

The constrained HFB calculations were carried out using the code `HFBaxial` written by one of us (L.M.R.). It uses a harmonic oscillator basis specified by the length parameters b_z and $b_\perp$ of the oscillator potential and the number of shells N_{osc} in the basis. For the calculations reported here we have taken a fixed spherical basis for all nuclei with oscillator length parameters $b_z = b_\perp = 2.1$ fm. The number of oscillator shells included in the basis is 10,12, and 14 for nuclei in the ranges $Z = [8, 50], [52, 82]$, and $[84, 100]$ respectively. This is more than enough to provide converged results for energy differences. We report on the results for the D1S Gogny interaction in sections below. More detailed results for the D1S as well as for other interactions of the Gogny form are given in the supplemental material [23].

III. EXAMPLES

In this section we will go through the details for four examples illustrating the application to a spherical nucleus, ^{208}Pb, a well-deformed nucleus, ^{158}Gd, the nucleus ^{226}Ra whose HFB ground state has a static octupole deformation, and a light nucleus having a very large

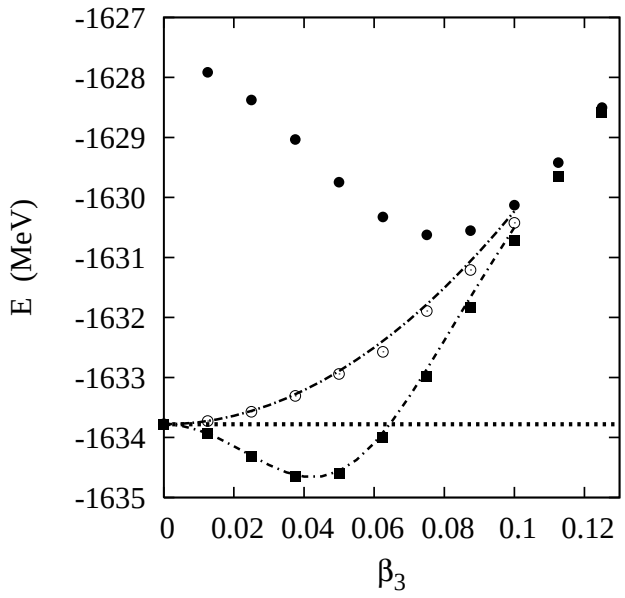

Figure 1: Energy of ^{208}Pb as a function of octupole deformation β_3. Open circles: HFB energy of constrained configurations ; Solid squares: energy E_e of the even-parity projected wave function; Solid circles: the odd-parity projected energy E_o. See the Appendix for explanation of the fitted lines.

transitional octupole moment, ^{20}Ne. A summary of the results for these nuclei is given in Table II at the end of this Section.

A. ^{208}Pb

The nucleus ^{208}Pb is a paradigm for a doubly magic nucleus. It is one of the very few nuclei whose first excited state has $J^\pi = 3^-$ quantum numbers. The excitation energy is 2.62 MeV and the transition rate is strongly collective with a strength of $B(E3,\uparrow) = 0.611$ e^2b^3 or 34 Weisskopf units[24]. For the theory, we first shown HFB and projected energies of the GCM configurations in Fig. 1. Note that the negative parity energy E_o is well defined in the limit $\beta_3 \to 0$ [3].

The minimum energy projected configurations, ie. the MAP states, are at $\beta_{3p} \approx 0.0375$ and $\beta_{3m} \approx 0.075$. One sees that the energy of the ground state is lower by projecting from a nonzero β_3; the associated correlation energy has the order of magnitude of one MeV. The MAP approximation to the excitation energy E_3 is given by the difference of the minima of

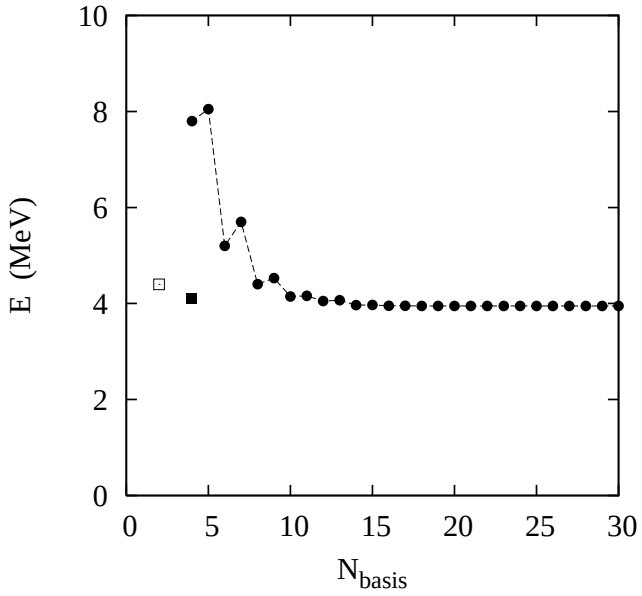

Figure 2: Excitation energy E_3 in ^{208}Pb as a function of the configuration space choice. Solid circles: HW using the singular value decomposition to keep N_{basis} states; solid square: HW with the two MAP states; open square: Energy difference of the two MAP states.

the plus- and minus-projected energy curves, which is about 4.2 MeV.

To see how the GCM calculated E_3 depends on the basis, we show it in Fig. 2 as a function of N_{basis}. The difference of MAP energies is the open square, and solid circles show the results with various truncations. The full basis set is comprised of the 41 configurations between $\beta_3 = -0.5$ to $\beta_3 = +0.5$ in steps of 0.025. The truncation is carried out by the singular-value decomposition.

One sees that the energy has converged at about $N_{basis} \approx 14$ and the numerics remain stable up to much larger values. The converged energy, 4.0 MeV, is fairly close to the difference of MAP energies. In fact, one can do even better in the 4-dimensional space allowing the MAP configurations to mix. This is shown as the solid square in the figure. We note that our excitation energy of 4.0 MeV is close to the value found in Ref. [2] using the GCM/HW method but with the Skyrme SLy4 interaction.

We see here that the MAP could be a very useful simplification, but its validity depends on the circumstances. It is also instructive to examine the GCM/HW wave function and compare it with MAP. These are shown in Fig. 3, for both the ground state and the odd-

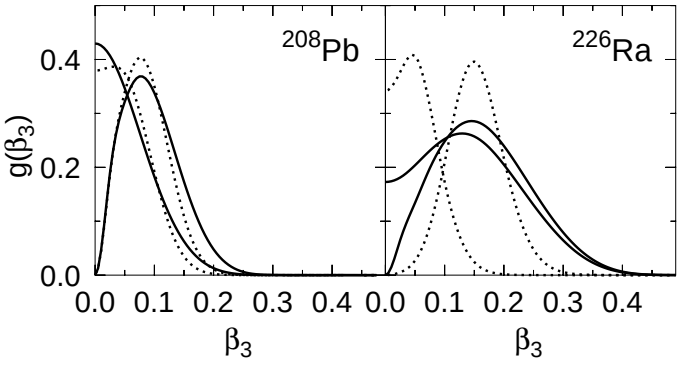

Figure 3: Wave function amplitudes. See text for explanation.

parity excited state. The wave function amplitudes are formally defined by the integral

$$g_\sigma(\beta_3) = \int d\beta_3' \mathcal{N}^{1/2}(\beta_3, \beta_3') f_\sigma(\beta_3') \tag{8}$$

where f is normalized $1 = \int d\beta_3\, d\beta_3' \mathcal{N}(\beta_3, \beta_3') f_\sigma(\beta_3') f_\sigma(\beta_3)$. The above relation establishes the connection between the standard GCM amplitudes f with the amplitudes g entering the expansion of the GCM wave functions in terms of orthogonal states $|q\rangle_{\rm orth} = \int dq' \mathcal{N}^{-1/2}(q, q')|q'\rangle$. The square root of the norm overlap is defined by the relation $\int dq'' \mathcal{N}^{1/2}(q, q'')\mathcal{N}^{1/2}(q'', q') = \mathcal{N}(q, q')$. The ground and excited state wave functions can be distinguished by the amplitude at $\beta_3 = 0$, which is finite for the even-parity ground state and zero for the odd-parity excited state. The HW wave function and the MAP approximation are shown as solid and dashed lines, respectively. It is clear that the MAP configuration is a good approximation to the full wave function of both the ground and excited states, for this particular nucleus.

More insight into the collective physics of the octupole degree of freedom can be obtained comparing with simple models of the excitation (See Appendix). If the configuration energies and interactions can be treated as quadratic functions of the deformation coordinate, and the matrix elements between different configurations can be treated by the GOA, the GCM/HW reduces to the RPA and is exact. The line through the HFB energy curve in Fig. 1 is a quadratic fit that reproduces well the computed energy. Also, the energy of the even-parity projected configuration follows well the predicted dependence according to the GOA, Eq. (16). This is shown as the line through the even-parity projected energies in the figure. Thus two of the conditions are met to reduce the GCM/HW theory to an RPA of a single collective state.

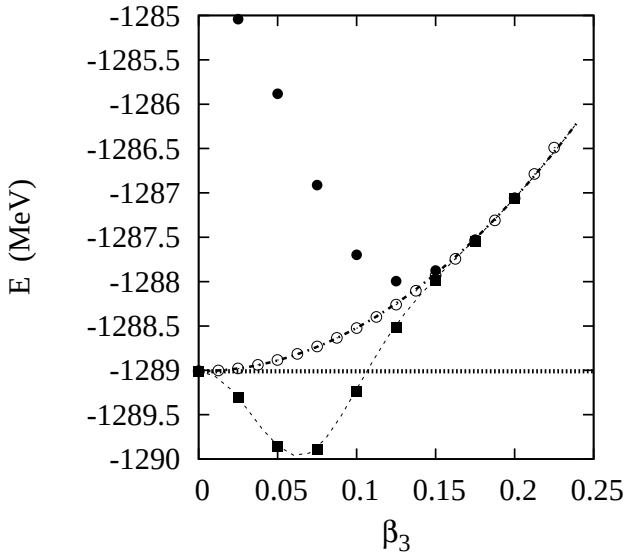

Figure 4: Energy of ^{158}Gd as a function of octupole deformation β_3. Open circles: HFB energy of constrained configurations ; Solid squares: energy E_e of the even-parity projected wave function; Solid circles: the odd-parity projected energy E_o. The line along the HFB values is the function $E_q = E_0 + K_1\beta_3^2$ with $K_1 = 48.8$ MeV fitted to the values $\beta_3 \leq 0.05$. The line along the E_e values is the fit motivated by the Gaussian overlap approximation, $E_e = E_q - K_2\beta^2/(1.0 + \exp(\alpha\beta^2))$, with K_2 and α fitted.

B. ^{158}Gd

Our example of a strongly deformed nucleus is ^{158}Gd. It has a 3^- excited state at 1.04 MeV with a transition strength $B(E3\uparrow) = 0.12$ e^{2}b^3. The energies from the GCM calculation are shown in Fig. 4. Overall, the energy curves look quite similar to those for ^{208}Pb. The HFB curve is also well fit by a quadratic dependence on β_3 but the curvature here is much shallower. The projected energy function $E_e(\beta_3)$ also has a similar shape to the curve for ^{208}Pb, and can be fitted by the same functional form, Eq. (14). The ratio of MAP minimum points is found to be $\beta_{3p}/\beta_{3m} \approx 2$, similar to the situation for ^{208}Pb. The excitation energy E_3 comes out to about 1.7 MeV, much smaller than the ^{208}Pb value. This is to be expected in view of the softer HFB curve. The correlation energy of the ground state, $E_0 - E_e$, is similar to the ^{208}Pb value, about one MeV.

Experimentally, the situation is complicated by the deformation and the splitting of the

octupole strength into different K-bands. There are three negative parity bands known experimentally at low energy. There is a $K = 1^-$ with an 1^- state at 977 keV, a $K = 0^-$ with the 1^- state at 1263 keV and finally a $K = 2^-$ with a 2^- state at 1793 keV. Our excitation energy of 1.7 MeV should be compared with the 1263 keV of the 1^- state of the $K = 0^-$ band. The theoretical value is stretched by a factor 1.4 with respect to the experimental value (see discussion below). Note that the measured octupole transition at 1.04 MeV is not relevant for the comparison because it corresponds to a different K value.

C. ^{226}Ra

^{226}Ra has the lowest 3^- excitation energy of any nucleus in the compilation of Ref [25], $E_3 = 320$ keV. It also has the highest transition strength in the compilation, $W(E3) = 54$ Weisskopf units[24]. On the theory side, the nucleus is predicted to deform both in the quadrupole ($\beta_2 \approx 0.3$) and the octupole degrees of freedom. The HFB/GCM energy curve, shown in Fig. 5, has a minimum at $\beta_3 \approx 0.13$.

This nucleus is very interesting for our survey, not only because of the static octupole deformation, but because the theory is seen to fail badly if the large amplitude fluctuations are not properly accounted for. The predicted excitation energies for different treatments of the GCM configurations are shown in Table I. The most naive theory (top line) would ignore the GCM construction and simply take the HFB minimum and project from that. The overlap $\langle -q|q\rangle$ at the HFB minimum is essentially zero and the E_3 comes out less than 1 keV. In the next approximation we consider (second line), we take the single configuration that gives the MAP ground state. Here the deformation is much closer to zero. However, the E_3 calculated as the difference between the even and odd projected states is now far too large, 1.7 MeV. Of course in the full MAP approximation we should take the configurations at different β_3 for odd and even projections. This is done in line 3 of the Table, and now the E_3 has the correct order of magnitude. Adding more configurations, the valued do not change much on an absolute MeV scale, but on a relative scale there is a considerable change. The most complete HW treatment, on the bottom line, underpredicts the energy by a factor of ≈ 2.

We also show the HW and MAP wave functions in Fig. 3. It is clear that the full wave functions are far from harmonic and that the MAP approximation fails badly.

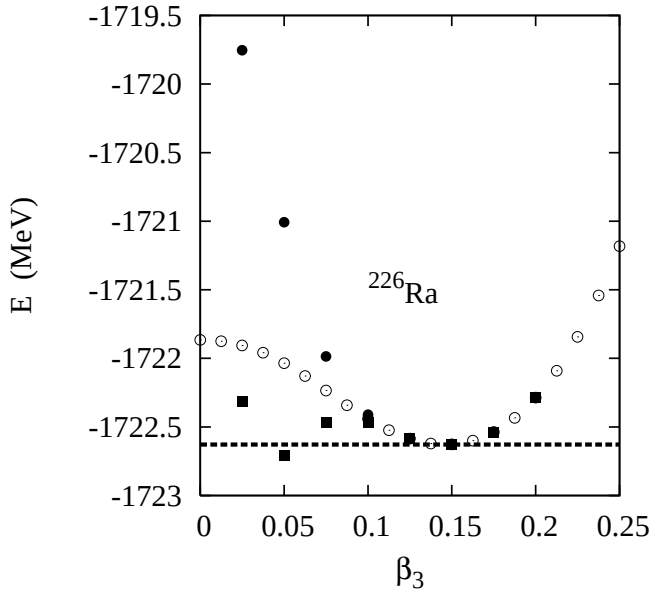

Figure 5: Energy of ^{226}Ra as a function of octupole deformation β_3 as in Figs. 1,4g. A very similar plot is shown in Fig. 3 of Ref. [3].

N_q	β_3	E_e (MeV)	E_o (MeV)	E_3 (MeV)
1	0.15	-1722.63	-1722.63	0.00
1	0.05	-1722.71	-1721.01	1.7
2	0.05, 0.15	-1723.43		0.37
3	0.05, 0.1, 0.15	-1723.45		0.31
4	0.025, 0.075, 0.125, 0.175	-1723.53		0.22
12	[-0.5,0.5]			0.16

Table I: Calculated energies of ^{226}Ra with various choices of the configuration set.

D. ^{20}Ne

^{20}Ne illustrates some differences that one sees in treating light nuclei by the GCM/HW, first studied by this method in Ref. [1]. Due to the incipient alpha clustering, the equilibrium octupole deformation of the projected configurations can be very large. The HFB and projected energies are shown in Fig. 6. Note that the HFB energy deviates from a quadratic dependence on the deformation, and looks almost linear at large β_3. Fig. 7 shows the density distribution at the two projected minima. One sees a compact localized density,

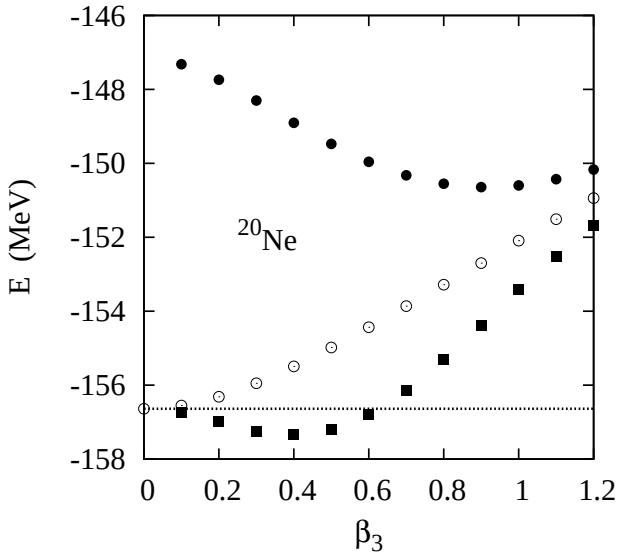

Figure 6: Energy of ^{20}Ne as a function of octupole deformation β_3 as in Figs. 1,4,5.

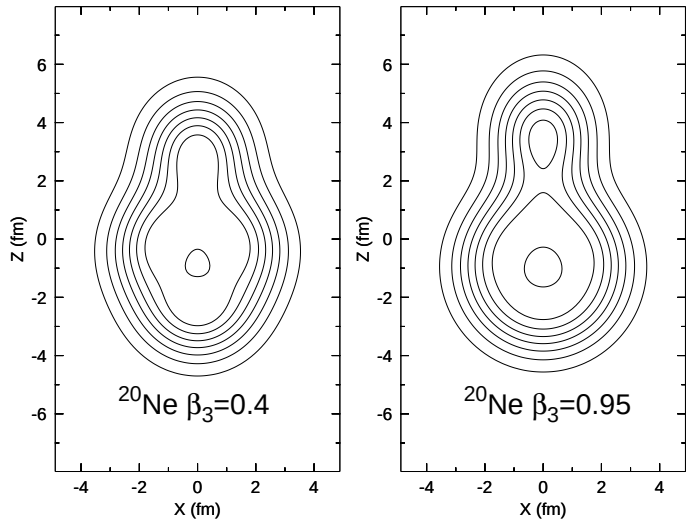

Figure 7: Nucleon density distribution in ^{20}Ne at β_{3p} (left) and β_{3m} (right).

suggestive of an alpha particle, outside a nearly spherical core. Since the alpha emission threshold is rather low in this nucleus, one should expect a softness in with respect to the generator coordinate corresponding to alpha cluster separation. In a multipole representation, this requires changing both the quadrupole and the octupole deformation. This is in fact what occurs in our GCM wave functions. Fig. 8 shows their deformations in the two multipolarities. The coupling of the multipolarities can cause problems, however. We will

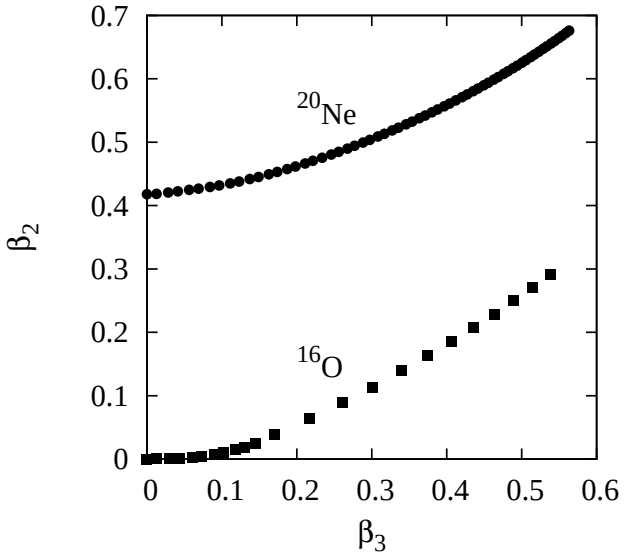

Figure 8: Deformation of the octupole-constrained HFB configurations for ^{16}O and ^{20}Ne.

come back to this in the Appendix, referring to the coupling in ^{16}O, also shown on the figure.

In table II the results for all the examples considered are collected. For the $B(E3)$ transition probabilities two formulas are used depending on the quadrupole deformation (see next section).

Nucleus	E_3 (MeV)			$W(E3)$		
	Exp.	Present	Other	Theory	Eq.	Exp.
^{20}Ne	5.6	6.7	5.2[a]	12	(11)	13
^{208}Pb	2.6	4.0	4.0[b]	53	(12)	34
^{158}Gd	1.04	1.93		11.6	(11)	12
^{226}Ra	0.32	0.16		43	(11)	54

Table II: Summary of results for the four examples discussed in the text. References for column 4, other theory: a) [1]; b) [2].

IV. SYSTEMATICS

We have applied the HFB/GCM/HW theory across the chart of nuclides including 818 nuclei between $8 \leq Z \leq 110$. About 6% of them are octupole deformed in the HFB ground

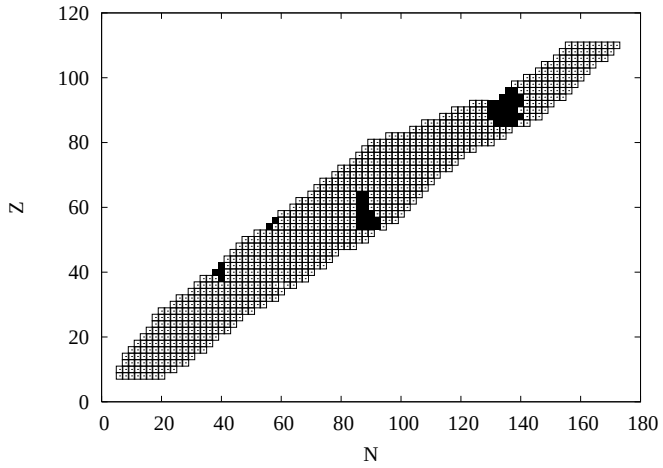

Figure 9: Chart of the nuclides showing those calculated in the present study. Those in black have static octupole deformations in HFB. Except for the nuclei near $N \sim Z \sim 40$, the nucleon numbers correspond well to the numbers 56, 88, and 136 listed in Ref. [10] as especially favorable for octupole deformation.

state. The nuclei are shown in Fig. 9. Favorable conditions for static octupole deformation occur when a high-j intruder orbital is close to an opposite-parity orbital with three units less of orbital angular momentum near the Fermi energy[10], which happens for Z and N values around 36, 56, 88, and 134. The regions around Ba and Ra are well-known in earlier studies. We also find static deformations near ^{80}Zr and near $Z \approx N \approx 56$ (for this region, see also Ref. [5]. There are also calculations in the literature reporting static octupole deformations in other regions as well[26, 27]. In any case, the HFB deformation is not an observable. Physically, one can only measure excitation energies and transitions strength. These are compared with experiment in the two subsections following.

A. Excitation energies

We now compare theory with the experimental data from the review by Kibédi and Spear [25]. The excitation energies of the 284 tabulated nuclei with $Z \geq 8$ are shown in Fig. 10, plotted as a function of A. The data show a strong overall A-dependence as well as shell-related fluctuations. The line shows a fit to the smooth trend in A with the phenomenological parameterization $E(A) = 103/A^{0.85}$ MeV. The most pronounced fluctuation about the trend is the rise and sudden drop near $A = 208$; the drop to low values is due to the extreme softness

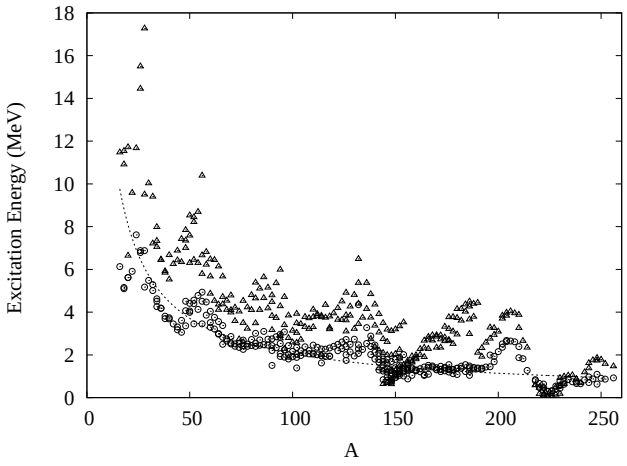

Figure 10: Octupole excitation energies as a function of mass number A. Circles: experiment; triangles: theory.

in the octupole mode. The theoretical energies, shown as triangles, replicate the overall trend with A and the dramatic fluctuation at $A \sim 208$. However, overall the theoretical energies are too high, particularly in the light nuclei.

A more detailed comparison of theory and experiment may be seen on the scatter plot Fig. 11. For excitation energies above 1 MeV, the theoretical values track the experimental but scaled by a factor. Around 1 MeV and below the theoretical values become closer to experiment. The lowest energy measured excitations are in the Ra isotopes, where the theoretical HFB wave functions have static octupole deformations. The theory reproduces the low energies to several hundred keV on an absolute energy scale, but does not do well on the logarithmic energy scale shown in the figure.

We also make some quantitative assessment of the performance of the theory, which should be useful in the future for comparing with other theories. We use the same performance measures as was used to assess theories of quadrupole excitations[11, 12], namely to compare ratios of theoretical to experimental quantities on a logarithmic scale. In terms of $R_E = \log(E(th)/E(exp))$ we determine the average value

$$\bar{R}_E = \langle R_E \rangle \tag{9}$$

and the dispersion about the average,

$$\sigma_E = \langle (R_E - \bar{R}_E)^2 \rangle^{1/2}. \tag{10}$$

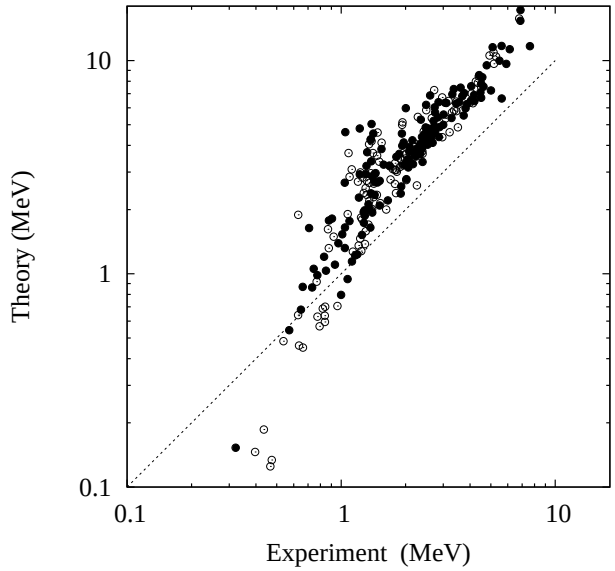

Figure 11: Octupole excitation energies, comparing the theory with experiment. Filled circles are excitations with measured $B(E3)$ strengths; open circles are other identified octupole transitions[25].

The results are shown in Table III. The first line shows the comparison taking the full HW treatment on the theoretical side and the full data set on the experimental side. One sees that the predicted energy is systematically too high, by a factor of $e^{0.44} \approx 1.6$. This is similar to the situation with the quadrupole excitations. There the understanding is that the wave function is missing components that would be included in collective theories using Thouless-Valatin inertial parameters. There may be other reasons for the systematic overprediction here that we will come back to in Sect. V. The dispersion in the values is $\sigma_E \approx 0.4$, corresponding to errors in the ratio of theory to experiment of -30% to $+50\%$. This is larger than the global dispersion found for the GCM-based theories of quadrupole excitations. However, we saw in Fig. 11 that there are differences in the nuclear structure that are responsible for the variable performance of the theory. Most importantly, the nuclei with calculated static octupole deformations should be treated separately. Taking out these nuclei, the dispersion decreases dramatically, as shown on the second line of the Table. A further distinction can be made between well-deformed and other nuclei, spherical and soft, respect to ordinary quadrupole deformations. A good theoretical indicator for deformed nuclei is the ratio of 4^+ to 2^+ excitation energies, called R_{42}. The values are available for

the Gogny D1S interaction from the global study[12], and we use them to set the condition $R_{42} > 2.9$ to define the set of well-deformed nuclei. The results are shown in the third and fourth rows of the table. One sees that the dispersion becomes even narrower for the nuclei in the nondeformed set. Thus, we can claim that the HFB/GCM/HW methodology is quite successful for nondeformed nuclei, when allowing for the overall scale factor. On the other hand, the deformed set is significantly poorer, with the average predicted energies higher and a larger dispersion. A possible cause of this poorer performance could be the misidentification of transitions in deformed nuclei. We have assumed here that all transitions are associated with the axially symmetric octupole operator ($K = 0$). As discussed in the next section, it is clear that some of the measured energies are for transitions with $K \neq 0$ (see also the ^{158}Gd example). Since all the K values in spherical nuclei are degenerate, this would explain the better overall agreement there.

		HW		MAP	
Selection	Number	$\bar{R}_e$	σ_e	$\bar{R}_e$	σ_e
all	284	0.45	0.40		
$\beta_3 = 0$	277	0.55	0.23	0.59	0.22
$\beta_3 = 0$, def.	59	0.62	0.32	0.75	0.26
$\beta_3 = 0$, sph.	196	0.52	0.19	0.53	0.17

Table III: Performance of the HW theory for excitation energies compared to the experimental data tabulated in Ref. [25]. The performance measures r_E and σ_E are given in Eq. (9) and (10) of the text. The performance of MAP is shown as well on lines 2-4 for subsets of nuclei selected by deformation criteria.

B. Transition strengths

The octupole transition strength is computed from the proton octupole transition matrix element $\langle o|\hat{Q}_3\frac{1+t_z}{2}|e\rangle$. In a strongly deformed nucleus, the excitation is in a $K = 0$ odd-parity band and the spectroscopic matrix element from the 3^- state in the band is given by

$$B(E3, 3^- \rightarrow 0^+) = \frac{e^2}{4\pi}\langle o|\hat{Q}_3\frac{1+t_z}{2}|e\rangle^2. \tag{11}$$

This formula was used in Ref. [3] to estimate the octupole transition strengths in Ra isotopes and other possible octupole-deformed nuclei. On the other hand, if the state $|e\rangle$ is spherical, then the excitation induced by Q_3 gives a state $|o\rangle$ that has good angular momentum and the transition strength can be calculated directly as

$$B(E3, 3^- \rightarrow 0^+) = \frac{7e^2}{4\pi}\langle o|\hat{Q}_3\frac{1+t_z}{2}|e\rangle^2. \tag{12}$$

Notice that this is a factor of 7 larger than Eq. (11). The reason for the difference is that Eq. (12) gives a total octupole transition strength, while Eq.(11) only gives the transition strength for the $K = 0$ components.

Besides these limiting cases, there are soft nuclei which should fall in between. Thus, it is imperative to restore good angular for the theory to have a global applicability. While angular momentum projection has been carried out in the past[28–30], it is beyond the scope of this article. Instead, we examine here the range of predicted values using a theoretical marker of the deformation to distinguish nuclei falling in the different categories. Fig. 12 shows the ratios of theoretical to experimental $B(E3)$ values, using the experimental data set from Ref. [25] and Eq. (11) for the theory. The data is plotted as a function of the quantity R_{42}, the ratio of the lowest 4^+ to 2^+ excitation energies. Values around 2 or less are characteristic of spherical nuclei, while strongly deformed nuclei have $R_{42} \geq 3$. We take the values for R_{42} from the spectroscopic calculations of Ref. [12], based on HFB/GCM with the same Gogny D1S interaction used for the theory here. The plot show a lot of scatter, but one can see two groups of nuclei, the left hand representing deformed nuclei. There is a trend visible in the $B(E3)$ ratios consistent with the above discussion.

To make the analysis more quantitative, we examine the logarithmic averages $\bar{R}$ dividing the nuclei into two groups according to R_{42}. The results are shown in Table IV. Since we use Eq. (11) to determine R, we should find $\bar{R} = 0$ for the first row of the Table. In fact, the average is about 40 % high. For the second row, if all the nuclei were spherical, the strength should be a factor of 7 larger. This implies that the $\bar{R}$ calculated with the deformed formula should give a value $0.33 - \log(7) = -1.6$. The value found, -0.99, shows that there is an important effect of the deformation but that it is too simplistic to assume that these nuclei are all spherical.

We note that the enhancement of the $B(E3)$ for the less deformed nuclei is evident in the projected calculations for ^{16}O ([28]) and Pb isotopes near $A = 208$ ([30]). Also, in Ref. [31]

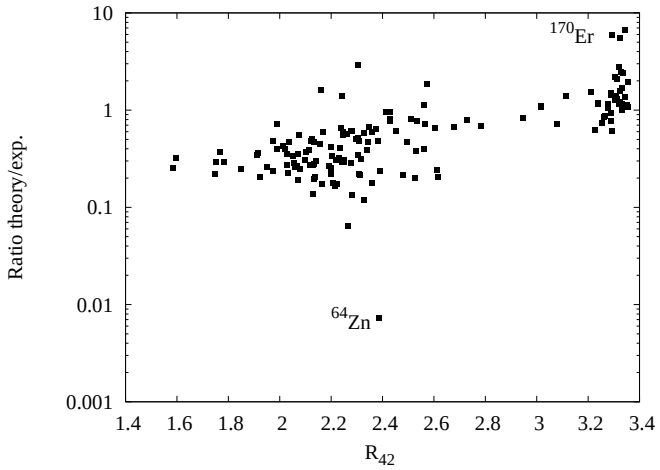

Figure 12: Ratio of theoretical octupole transition strength to experimental, with the theoretical strength obtained using Eq. (11). The horizontal axis is the ratio R_{42} from the theory of Ref. [12]. Experimental $B(E3)$ values are from Ref. [25].

Selection	Number	$\bar{R}$	σ
Deformed, $R_{42} > 2.9$	41	0.34	0.5
Other, $R_{42} < 2.9$	112	-0.99	0.7

Table IV: Ratio of theoretical to experimental $B(E3)$ strengths. The second column is the number of nuclei in the data set.

the authors remark on a strong disagreement between theory and experiment for ^{96}Zr. This is the case if one uses Eq. (11), but that nucleus is spherical according to the R_{42} criterion and Eq. (12) gives a satisfactory agreement. We note also that ^{96}Zr was predicted to be unstable with respect to octupole deformations in Ref. [32].

It is of interest to examine the nuclei that deviate most strongly from the theory. In Fig. 12 there is a group of three outlier nuclei in the upper right-hand corner. The nuclei are ^{170}Er and its neighbors. In these cases, the experimental transitions are likely to be to excited states with $K \neq 0$. The lowest 1^- excitation in ^{170}Er at 1.26 MeV has a $K = 1^-$ character, and the first $K = 0^-$ is higher by 0.6 MeV. There are some studies in the literature in which the K-dependence of the octupole excitation is examined[4, 33, 34]. In Ref. [33, 34] the $K = 0^-$ bands were found to be higher in energy than other K values.

The other glaring anomaly is the nucleus ^{64}Zn at $R_{42} \approx 2.4$, which has a grossly under-

predicted $B(E_3)$. It turns out that the quadrupole deformation of this nucleus changes sign as β_3 is increased. The ground state at $\beta_3 = 0$ is oblate, but it switches to another minimum with a prolate shape at moderate values of β_3. The very small predicted $B(E3)$ is due to the small overlap between the oblate and prolate configurations. Clearly, the GCM must include explicitly both quadrupole and octupole degrees of freedom to properly treat this nucleus. A few other nuclei with similar Z values show the same behavior. We note that the $B(E3)$ comes out much closer to experiment if both even and odd states are taken from configurations having the same sign of quadrupole moment.

V. DISCUSSION

We have demonstrated that a global theory of the octupole degree of freedom can be constructed using the HFB/GCM/HW methodology. The theory reproduces the secular trend of the excitations, the effects of an incipient static octupole deformation, and the most visible shell effects. However, the theory has obvious deficiencies. Most notably, we require a overall scaling factor of 1.6 to make quantitative comparison with experiment. It is urgent to understand what physics is needed to make predictions on an absolute energy scale. There are several possible reasons for the absolute errors. One is the Hamiltonian itself. Besides the Gogny interaction, there have been calculations with the BCP interaction, interactions from the Skyrme family and from relativistic mean-field theory. Ref. [17] found that the D1S Gogny interaction and the BCP interaction gave significant differences in the odd-parity excitations of Ra isotopes. The Gogny interaction is guided by nuclear Hartree-Fock theory, and one of the characteristics is a nucleon effective mass less than the physical mass. This implies that single-particle excitation energies will be higher than for a non-interacting system, and these effects could carry over to the collective excitations as well. We note that the calculation of the ^{208}Pb in Ref. [2] using a Skyrme interaction with a similar effective mass to D1S agrees with our results. However, the Relativistic Mean Field Hamiltonian also has a small effective mass, but excellent agreement was obtained for E_3 in an isotone chain by (Q)RPA [9].

This brings up another source of systematic error in the GCM/HW, the restriction of the degrees of freedom in the excitation to a single variable. It is well-known in the theory of quadrupole excitations that time-odd components must be included in the wave func-

tion to obtain good moments of inertia[38]. For large amplitude deformations, this can be achieved by self-consistent cranking. When no time-odd components are allowed in the angular momentum projected (AMP) GCM calculation the excitation energy is stretched with respect to standard cranking calculations by a factor of around 1.4. This correction factor is compatible with the discrepancies observed between our results and the experiment in the case of ^{158}Gd as well as with the overall 1.6 factor for the negative parity excitation energies discussed previously. The single-operator approximation is also problematic due to the fragmentation of octupole strength in the full spectrum. Roughly speaking, the octupole strength has two important branches: the low collective excitation that is under study here, and the high-lying excitation characterized as $3\hbar\omega$ in the harmonic oscillator model. Our generating field introduces amplitudes of both into the constrained wave function.

More generally, one can introduce methods that would reduce to (Q)RPA in the small amplitude limit. The raises the question of how well (Q)RPA would perform in a global context. As shown in the Appendix, for a large fraction of nuclei the GCM/HW methodology is essentially equivalent to (Q)RPA in a single collective variable. For these nuclei, the (Q)RPA is justified and is very likely to give lower excitation energies.

The interaction of the octupole with the quadrupole degree of freedom is an interesting problem that appears in several contexts in our study. First, the HFB static quadrupole deformation of many nuclei invalidates a spectroscopic interpretation of the observables for the physical angular momentum eigenstates of the system. We saw this most directly in the discussion of the $B(E3)$ transition strengths. The solution is to carry out angular momentum projection. Another aspect missing from our study is the inclusion of $K \neq 0$ excitations in deformed nuclei. This has been done in HFB-BCS in Ref. [4, 33, 39] and in HFB in Ref. [34]. Since $K \neq 0$ bands can fall below the $K = 0$ octupole excitation band, it is essential for a complete theory of the octupole excitations in deformed nuclei. We note that collective models can be constructed that provide formulas relating the quadrupole excitation energies to the octupole energies, and octupole energies to the $B(E3)$ transition strengths [35, 36]. The interaction between quadrupole and octupole degrees of freedom might also play a role in parity-violating transitions [37].

Some aspects of the quadrupole-octupole mixing may require a two-dimensional GCM to describe properly. It was clear in the light nuclei that octupole and quadrupole deformations are strongly coupled in forming alpha-clusters. Also we found that the severe problem

describing the $B(E3)$ in ^{64}Zn could be traced to the coupling. We note that the two-dimensional GCM has been implemented in the past. In Refs. [14] the coupled GCM was applied to the complex spectroscopy of the nucleus ^{194}Pb. Also, the microscopic theory of asymmetric fission[13] requires at least a two-dimensional GCM.

One last aspect of the theory should be mentioned. We have seen in the examples that the correlation energy of the ground state associated with the $K = 0$ octupole excitation is of the order of one MeV. This can have an important influence on the theory of the nuclear masses. We plan to investigate the systematics of the correlation energy in a future publication.

VI. ACKNOWLEDGMENTS

We thank H. Goutte, P.-H. Heenen, and W. Nazarewicz for reading and comments on the manuscript, as well as V. Zelevinsky and N. Auerbach for communications. This work was supported in part by the U.S. Department of Energy under Grant DE-FG02-00ER41132, and by the National Science Foundation under Grant PHY-0835543. The work of LMR was supported by MICINN (Spain) under grants Nos. FPA2009-08958, and FIS2009-07277, as well as by Consolider-Ingenio 2010 Programs CPAN CSD2007-00042 and MULTIDARK CSD2009-00064.

[1] S. Marcos, H. Flocard, and P.H. Heenen, Nucl. Phys. **A410** 125 (1983).

[2] P.-H. Heenen, et al., Eur. Phys. J. A **11** 393 (2001).

[3] J.L. Egido and L.M. Robledo, Nucl. Phys. **A524** 65 (1991).

[4] J. Skalski, et al., Nucl. Phys. **A551** 109 (1993).

[5] P.-H. Heenen, et al., Phys. Rev. C **50** 802 (1994).

[6] E. Garrote, J.L. Egido, and L.M. Robledo, Phys. Rev. Lett. **80** 4398 (1998).

[7] A.P Severyukhin, C. Stoyanov, V.V. Voronov, and N. Van Giai, Phys. Rev. C**66** 034304 (2002).

[8] G. Colò, et al., Nucl. Phys. **A722** 111c (2003).

[9] A. Ansari and P. Ring, Mod. Phys. Lett. A **24** 3103 (2009).

[10] P.A. Butler and W. Nazarewicz, Rev. Mod. Phys. **68** 349 (1996).

[11] B. Sabbey, M. Bender, G.F. Bertsch, and P.-H. Heenen, Phys. Rev. C 75, 044305 (2007).

[12] J.-P. Delaroche, et al., Phys. Rev. C **81** 014303 (2010).

[13] H. Goutte, J.F. Berger, P. Casoli, and D. Gogny, Phys. Rev. C **71** 024316 (2005).

[14] J. Meyer, et al., Nucl. Phys. **A588** 597 (1995).

[15] S. Péru and H. Goutte, Phys. Rev **C 77**, 044313 (2008)

[16] R. Rodríguez-Guzmán, J.L. Egido and L.M. Robledo, Nucl. Phys. **A709**, 201 (2002)

[17] L.M. Robledo, et al., Phys. Rev. C **81** 034315 (2010).

[18] In the present application, there is no phase ambiguity in applying the Onishi formula because the configurations are time-reversal invariant.

[19] R. Balian and E. Brezin, Nuovo Cimento B**64** 37 (1969).

[20] P. Bonche, J. Dobaczewski, H. Flocard, P. -H. Heenen, and J. Meyer, Nucl. Phys. **A 510**, 466 (1990)

[21] L.M. Robledo, Intl. J. of Mod. Phys. **E 16**, 337 (2007).

[22] L.M. Robledo, J. Phys. G **37** 064020 (2010).

[23] If accepted by Phy. Rev. C, the files will be accessible in the supplementary data accompanying the article.

[24] The transition strength in Weisskopf units $W(E3)$ is given by the formula $W(E3) = 2.404 \times 10^6 B(E3,\uparrow)/A^2$.

[25] T. Kibédi and R. Spear, Atomic Data and Nuclear Data Tables **80** 35 (2002); R.H. Spear, Atomic Data and Nuclear Data Tables **42** 55 (1989).

[26] P. Möller, R. Bengtsson, et al., At. Data Nucl. Data Tables **94** 758 (2008).

[27] W. Zhang, Z. Li, Q. Zhang, and J. Meng, Phys. Rev. C **81** 034302 (2010).

[28] J.L. Egido, L.M. Robledo, and Y. Sun, Nucl. Phys. **A560** 253 (1993).

[29] Y. Sun, L.M. Robledo, and J.L. Egido, Nucl. Phys. **A570** 305c (1994).

[30] J.L. Egido, V. Martin, L.M. Robledo, and Y. Sun, Phys. Rev. C **53** 2855 (1996).

[31] J. Skalski, P.-H. Heenen, P. Bonche, Nucl. Phys. **A559** 221 (1993).

[32] A. Abbas, N. Auerbach, N. Van Giai, and L. Zamick, Nucl. Phys. **A367** 189 (1981).

[33] K. Zberecki, P. Magierski, P.-H. Heenen, and N. Schunck, Phys. Rev. C **74** 051302 (2006).

[34] M. Yamagami, K Matsuyanagi, M.Matsuo, Nucl. Phys. **A693** 579 (2001).

[35] M. Metley, et al., Phys. Rev. C **52** 1801 (1995).

[36] W. Mueller, et al., Phys. Rev. C **73** 014316 (2006).

[37] V. Flambaum and V. Zelevinsky, Phys. Rev. C 68, 035502 (2003)

[38] R. Rodríguez-Guzmán, J.L. Egido and L.M. Robledo, Phys. Rev. **C62**, 054319 (2000)

[39] H. Dancer et al., Nucl. Phys. **A654** 655 (1999).

[40] P. Ring and P. Schuck, "The Nuclear Many-Body Problem", (Springer, NY), 1980, Sec. 10.7.5.

[41] L.M. Robledo, Phys. Rev. C**46** 238 (1992).

[42] K. Hagino and G.F. Bertsch, Phys. Rev. C **61** 024307 (2000).

[43] D.M. Brink and A. Weiguny, Nucl. Phys. **A120** 59 (1968).

[44] Another more restricted derivation is given by B. Jancovici and D.H. Schiff, Nucl. Phys. **58** 678 (1964).

Appendix: Simplified approximations and limits

It is important to understand the limiting behavior of any computationally demanding theory, both to check the reliability of the calculations as well as to see whether approximations are justified that would simplify the calculations. For the GCM/HW methodology, the theory becomes analytic or nearly so if a few conditions are met. One requirement is that there be only a single degree of freedom necessary to describe the excitation of the system. There are simple Hamiltonians that satisfy this condition. Examples are the Lipkin model[40], [41], where the degree of freedom is the number of particles in the excited orbital, and the two-particle problem treated in Ref. [42] where the degree of freedom is the center-of-mass displacement. In the last model and other like it the theory becomes analytic and reduces to the RPA if the overlap integrals satisfy the Gaussian Overlap Approximation and the matrix elements of the Hamiltonian reduce to a quadratic functions times the overlap. In fact the relation to RPA remains even if there are many degrees of freedom in the GCM [43, 44].

To make the discussion concrete, let us assume that there is a single continuous degree of freedom q and we can write the overlap integral and the Hamiltonian matrix element as

$$\langle q'|q\rangle = e^{-(q-q')^2/q_s^2} \tag{13}$$

$$\frac{\langle q'|H|q\rangle}{\langle q'|q\rangle} = E_0 + \frac{1}{2}v(q+q')^2 - \frac{1}{2}w(q-q')^2 \tag{14}$$

The solution obtained by the Hill-Wheeler construction is identical to the solution of the RPA equation for the operator $\hat{Q}$ that generates the GCM states $|q\rangle$. The HW wave functions

have the form of Gaussians in the variable q and the excitation energy is given by

$$\hbar\omega_{RPA} = q_s^2\sqrt{vw}. \tag{15}$$

Let us now compare with the MAP approximation. Here one first calculates projected energies as a function of q,

$$\frac{\langle e|H|e\rangle}{\langle e|e\rangle} = 2vq^2\frac{v - we^{-4(q/q_s)^2}}{1 + e^{-4(q/q_s)^2}} \tag{16}$$

and

$$\frac{\langle o|H|o\rangle}{\langle o|o\rangle} = 2vq^2\frac{v + we^{-4(q/q_s)^2}}{1 - e^{-4(q/q_s)^2}} \tag{17}$$

The energies are then minimized with respect to q. The results for a range of values of the ratio w/v are given in Table V. The ratios q_0/q_e are close to $\sqrt{3}$, which may reflect the harmonic oscillator character of the exact HW wave functions. In the last columns we compare the MAP excitations energy with the RPA values. They are remarkably close.

w/v	q_e	E_e	q_o	E_o	$E_o - E_e$	$\hbar\omega_{RPA}$
1.5	0.226	-0.0125	0.390	1.212	1.225	1.225
2.0	0.292	-0.0421	0.509	1.373	1.415	1.414
4.0	0.400	-0.232	0.716	1.782	2.01	2.00
8.0	0.469	-0.721	0.870	2.207	2.93	2.83

Table V: The MAP solution in the harmonic limit. Deformations are in units of q_s and energies are in units of vq_s^2. The last column shows the (Q)RPA excitation energy, Eq (15).

As a general conclusion, we find that if the MAP conditions are satisfied, the energies are close to the RPA performed with a single collective variable. For those nuclei, it would better to extend the space for the calculation using more RPA degrees of freedom than by going to large amplitudes in a single collective variable.

It would be nice to find a criterion to test for validity of the simplified treatment. The first condition we can check is the ratio q_o/q_e. This is graphed in Fig. 13 for the 284 nuclei tabulated in Ref. [25].

There is a strong peak at $\beta_{3m}/\beta_{3p} \approx 1.9$. This is slightly higher than the single-mode (Q)RPA, but still close enough to make a further investigation of the quadratic Hamiltonian

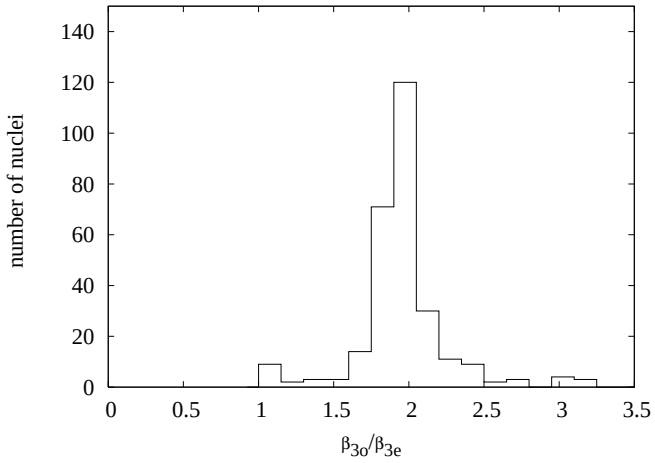

Figure 13: Ratio of MAP deformations β_{3p}/β_{3m} for nuclei with measured E_3 [25].

approximation. There are also wings on the distribution extending from 0.9 (^{16}O) to 3.2 (^{230}U). Excluding the wings below 1.7 and above 2.2, the peak contains 80 % of the measured nuclei.

To examine the validity of the quadratic approximation, we compared the extracted coefficients vq_s^2 and wq_s^2 at the two deformations β_{3p} and β_{3m}. If the quadratic approximation is valid, they should be equal. For example, the values of β_{3p} and β_{3m} at the closest mesh points are 0.0375 and 0.075, respectively. The values of $v\beta_{3p}^2$ and $w\beta_{3p}^2$ extracted at that mesh point are 0.23 MeV and 1.72 MeV, respectively. The corresponding numbers for β_{3m} are 0.94 MeV and 7.20 MeV, very close to 4 times the values at β_{3p}. This is just what is expected given $\beta_{3m}/\beta_{3p} = 2$, showing that ^{208}Pb satisfies the conditions for the quadratic Hamiltonian. With these values for v and w, the RPA energy formula Eq. (15) gives 3.9 MeV, close to the GCM/HW value of 4.0 MeV. The results for the nuclei within the peak of Fig. 14 is shown as a scatter plot of the ratios. In general, the w term follows a quadratic dependence very well. The v term can have large deviations, particularly for nuclei that are soft to octupole deformations. However, for most of the nuclei, the quadratic approximation is valid to an accuracy far better than needed, given the overall performance of the theory in non-octupole deformed nuclei at the 25% level in the scaled energies.

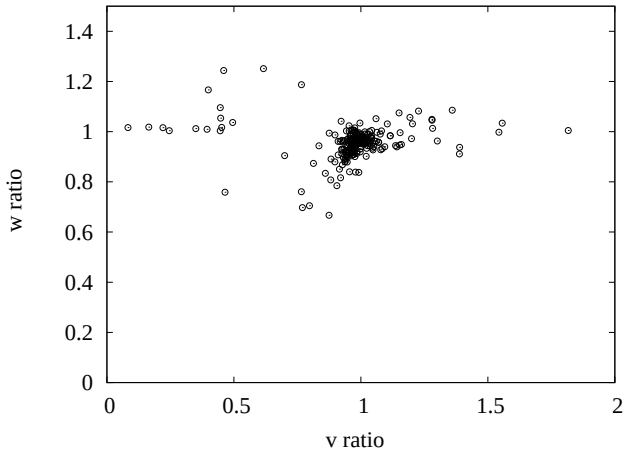

Figure 14: Ratio of MAP deformations β_{3m}/β_{3p} for nuclei with measured E_3 [25].